Frequency dependence of the thermal conductivity of semiconductor alloys

Yee Kan Koh and David G. Cahill
Department of Materials Science and Engineering and Frederick Seitz Materials Research Laboratory, University of Illinois, Urbana, Illinois 61801, USA
(Received 14 May 2007; published 23 August 2007)

The distribution of phonons that carry heat in crystals has typically been studied through measurements of the thermal conductivity Λ as a function of temperature or sample size. We find that Λ of semiconductor alloys also depends on the frequency of the oscillating temperature field used in the measurement and hence demonstrate a novel and experimentally convenient probe of the phonon distribution. We report the frequency dependent Λ of $In_{0.49}Ga_{0.51}P$, $In_{0.53}Ga_{0.47}As$, and $Si_{0.4}Ge_{0.6}$ as measured by time-domain thermoreflectance over a wide range of modulation frequencies $0.1<f<10$ MHz and temperatures $88<T<300$ K. The reduction in Λ at high frequencies is consistent with a model calculation that assumes that phonons with mean free paths larger than the thermal penetration depth do not contribute to the thermal conductivity measured in the experiments.

DOI: 10.1103/PhysRevB.76.075207 PACS number(s): 66.70.+f, 44.10.+i, 63.90.+t, 81.70.Pg

I. INTRODUCTION

In crystalline dielectrics and semiconductors, heat is carried by wavelike lattice vibrations, i.e., phonons, with a broad distribution of frequencies and lifetimes.[1] In a typical crystal near room temperature, the spectral distribution of the thermal conductivity Λ is thought to be nearly flat[2] because the variation of the density of states with phonon frequency, ν^2 in the Debye model, is compensated by changes in phonon lifetimes, typically assumed to scale as ν^{-2}. In mixed crystals such as the semiconductor alloys used in thermoelectric energy conversion, Rayleigh scattering of high-frequency phonons shifts the distribution and increases the relative importance of low-frequency phonons for heat transport.[2]

Current research on improving the efficiency of thermoelectric materials is often concerned with understanding this phonon distribution and developing material structures, e.g., nanowires, superlattices, and nanoscale precipitates, that further reduce the thermal conductivity Λ below which can be achieved by alloying.[3–5] Currently, the most powerful methods for probing the distribution of phonon mean free paths are systematic experiments on how Λ measured under steady-state conditions[3,6] varies as a function of the diameter of a nanowire or the thickness of a crystalline layer. In this paper, we report our observation of frequency dependence of Λ for semiconductor alloys and thus demonstrate an alternative and convenient method for profiling the distribution of heat carrying phonons in materials.

Frequency or time dependence of Λ has been discussed by theorists for many years but the expectation has usually been that very high frequencies $f>1/\tau$, where $1/\tau$ is the relaxation rate of the dominant phonons, would be needed to observe these effects. (One notable exception is the study by Mahan and Claro who found changes in the heat current when the temperature gradient varies rapidly on the length scale of the phonon mean free path.[7]) Guyer and Krumhansl,[8] for example, predicted a correction to the static thermal conductivity on the order of $2\pi f\tau_R$, where τ_R is the mean relaxation time due to resistive scattering processes. More recently, Volz[9] showed that Λ in a computational model of Si decreases at frequencies $f\tau>1$. Since the lifetimes of the dominant phonons in semiconductor alloys are $\sim$100 ps, this prior theoretical work suggests that the frequency dependence of Λ would not be observable in experiment unless $f>1$ GHz.

In our experiments, we observe frequency dependence in Λ for semiconductor alloys when $f>1$ MHz. This surprising result is consistent with a model based on the assumption that phonons with mean free paths greater than the thermal penetration depth, $\boldsymbol{d}=\sqrt{\Lambda/\pi Cf}$, where C is the heat capacity per unit volume, do not contribute to Λ measured in the experiments. Thus, by varying f and therefore $\boldsymbol{d}$, we conveniently probe the distribution of phonon mean free paths. Our results also have practical importance in the design and thermal management of microelectronics: InGaP, InGaAs, and SiGe are common in high-frequency devices[10,11] and our finding that Λ is dependent on both the layer thickness and the time scale of the heat transport creates challenges for accurate modeling of temperature distributions in these devices.[12]

II. EXPERIMENTAL DETAILS

InGaP and InGaAs samples, supplied by Epiworks Inc., were epitaxially grown on GaAs and InP substrates, respectively, by metal organic chemical vapor deposition (MOCVD). The 70 nm InGaP epitaxial layer was obtained by sequential selective etching of GaAs and InGaP from a multilayer HBT InGaP/GaAs wafer, also grown by MOCVD. The $Si_{0.4}Ge_{0.6}$ sample was provided by Professor Fitzgerald of MIT.[13] The layer thickness of the samples is measured by picosecond acoustics. The longitudinal speed of sound is 5.22 nm ps^{-1} in InGaP and 4.25 nm ps^{-1} in InGaAs, derived from the average of the speed of sound in the pure crystals.[14] InGaP samples (2007, 178, and 70 nm) are undoped, except the 456 nm layer, which is lightly doped (n type, 2.5×10^{17} cm^{-3}). The InGaAs samples have a range of dopant concentrations: n type, 10^{15} cm^{-3} (3330 nm); p type, 2.3×10^{19} cm^{-3} (891 nm); p type, 2.7×10^{19} cm^{-3} (591 nm);

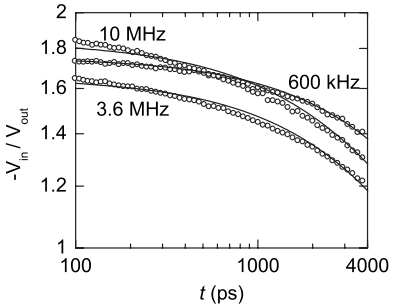

FIG. 1. Fits of the thermal model (solid lines) to the TDTR measurements (open circles) used to determine the thermal conductivity of a 2010 nm thick InGaP layer at various frequencies. In these fits, the thermal conductance of the Al/InGaP interface is fixed for all three curves at $G=51$ MW m^2 K^{-1}. The curves are labeled by the modulation frequency of the pump laser, V_{in} and V_{out} are the in-phase and out-of-phase signals of the rf lock-in amplifier that detects the small changes in the intensity of the reflected probe beam produced by the pump, and t is the time delay between the pump and probe optical pulses.

and p type, 9×10^{18} cm^{-3} (431 nm). The 6000 nm SiGe sample is undoped. To prepare the samples for measurements, we deposit 70–100 nm thick Al films by magnetron sputter deposition.[15]

We measure the thermal conductivities by time-domain thermoreflectance (TDTR).[16,17] A schematic diagram of our equipment is given in Ref. 18 and our method for data analysis is described in Ref. 19. In our TDTR measurements, a laser beam from a mode-locked Ti:sapphire is split into a pump beam and a probe beam with the relative optical path being adjusted via a mechanical delay stage. The pump beam is modulated at a frequency f in the range $0.1<f<10$ MHz. The radii of the laser beams are 6.5–15 μm at the sample surface. We use beam powers of 5–24 mW, creating temperature rises of <7 K. For measurements at frequencies lower than 0.6 MHz, we use a pulse picker to reduce the laser repetition rate to 5 MHz. The extinction ratio of the pulse picker is 1:200; the residual leakage of pulses at 80 MHz is accounted for in the thermal model.

We use a numerical solution of the diffusion equation in cylindrical coordinates to model the thermal responses of our samples.[19] Instead of the conventional in-phase signal analysis, the ratio of in phase and out of phase of the lock-in amplifier is used in our analysis to take advantage of the extra information in the out-of-phase signal. As a refinement over the procedure described in Ref. 19, we employ a time-weighted average of the model predictions for the starting and ending radii of the laser beams to account for changes in the radius of the pump beam as function of the position of the optical delay line. Heat capacities are taken from literature values. The thermal model has two free parameters, the thermal conductance of the Al/semiconductor interface and Λ of the semiconductor layer. These parameters are adjusted to give the best fit between the model and the measurements, see Fig. 1.

III. RESULTS AND DISCUSSION

To a good approximate, the in-phase signal of the lock-in amplifier V_{in} gives the time-domain response of the surface temperature following heating by the pump optical pulse.[19] At $t=100$ ps, heat is uniformly distributed through the Al metal film but the amount of heat that has entered the semiconductor layer at this short time scale is relatively small. Therefore, the change in V_{in} between negative delay time and $t=100$ ps is determined by the heat capacity per unit area of the Al film and is proportional to $1/(h_{\mathrm{Al}}C_{\mathrm{Al}})$, where h_{Al} is the thickness of the Al film and C_{Al} is the heat capacity per unit volume of Al. V_{out}, on the other hand, is predominately controlled by the imaginary part of the frequency domain response of the surface temperature subjected to a periodic heat source of frequency f. For thick samples with intermediate thermal conductivity, V_{out} is proportional to $(\Lambda C f)^{-1/2}$, where Λ is the thermal conductivity of the samples, C is the heat capacity per unit volume of the samples, and $(\Lambda C)^{1/2}$ is the thermal effusivity. (For high thermal conductivity materials at low f, V_{out} is suppressed by radial heat flow around the focused laser spot; for low thermal conductivity materials at high f, V_{out} is suppressed by the heat capacity of the Al thin film transducer.) Hence, at intermediate time (100–500 ps), our TDTR measurements are most sensitive to the thermal effusivity of our samples.

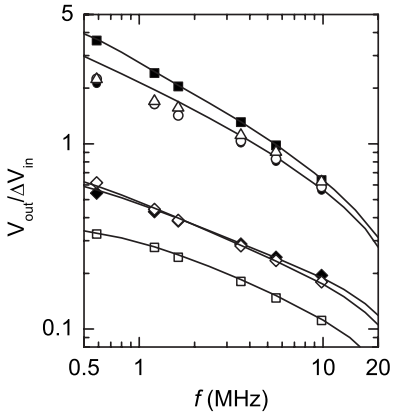

FIG. 2. Frequency dependence of the out-of-phase signal normalized by the jump in the in-phase signal. Measured $V_{out}/\Delta V_{in}$ of Si (open squares), SiO_2 (solid squares), GaAs (open diamonds), InP (solid diamonds), InGaP (open circles), InGaAs (solid circles), and $Si_{0.4}Ge_{0.6}$ (open triangles) are compared to the respective calculations from the thermal model (solid lines), from top to bottom, of SiO_2, semiconductor alloys, GaAs, InP, and Si. For calculation of semiconductor alloys, we assume $\Lambda=3$ W m^{-1} K^{-1}, $C=1.69$ J cm^{-3} K^{-1}, and Al film thickness of 93 nm. Only measurements of semiconductor alloys deviate from the calculations.

In Fig. 2, we plot the out-of-phase signal of the lock-in amplifier V_{out} normalized by the change in the in-phase signal ΔV_{in} between a negative delay time and a positive delay time of $t=100$ ps as a function of modulation frequency f. ΔV_{in} can be thought of as a calibration for V_{out} that is based on the heat capacity per unit area of the Al transducer. $V_{out}/\Delta V_{in}$ is thus proportional to the reciprocal of thermal effusivity of the samples. For all materials we have studied except thick layers of semiconductor alloys, a single value of the thermal effusivity is sufficient to fit the entire frequency range of the data acquired at room temperature, see Fig. 2. For InGaP, InGaAs, and SiGe, however, the measurements

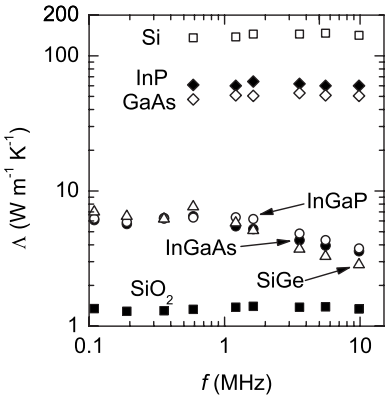

FIG. 3. Room temperature thermal conductivity of single crystals of Si, InP, and GaAs; a 1 μm thick layer of amorphous SiO_2; and epitaxial layers of semiconductor alloys as a function of the modulation frequency used in the measurement. Data for 2010 nm thick InGaP, 3330 nm thick InGaAs, and 6000 nm thick $Si_{0.4}Ge_{0.6}$ are shown as open circles, filled circles, and open triangles, respectively.

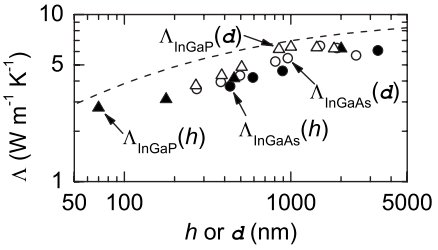

FIG. 4. Comparison of the frequency and thickness dependences of the room temperature thermal conductivity of III-V semiconductor alloys. Data for 2010 nm InGaP (triangles) and 3330 nm InGaAs (circles) acquired at different frequencies (open symbols) are plotted as a function of penetration depth, $\boldsymbol{d}=\sqrt{\Lambda/\pi Cf}$, where Λ is thermal conductivity of thick layers at low frequency, C is the heat capacity per unit volume, and f is the modulation frequency. Also included are data for epitaxial layers of different thicknesses measured at low f with $\boldsymbol{d}>h$ (filled symbols) plotted as a function of the layer thickness h. The dashed line is the calculated thermal conductivity using the isotropic continuum model described in the text for InGaAs that limits the mean free path of the phonons to the layer thickness.

cannot be fitted by a single value of the thermal effusivity. When a thermal conductivity of $\Lambda=3$ W m^{-1} K^{-1} is chosen to fit the data for $V_{out}/\Delta V_{in}$ in the high-frequency limit, the data at low f fall below the predictions of the thermal model by a factor of $\sim$0.7 implying that thermal conductivity is a factor of $\sim$2 larger at lower f.

We analyze the data quantitatively by fitting the calculations of a diffusive model to our measurements. Since we do not expect that the thermal conductance of the interface between the Al film and the samples depends on heating frequency, we fix the thermal conductance and vary the thermal conductivity of the samples as the only free parameter. Typical examples of this fitting procedure are shown in Fig. 1. We summarize the thermal conductivity Λ measured in this way as a function of the modulation frequency f in Fig. 3. As already indicated by the data shown in Fig. 2, the thermal conductivity for all materials we have studied except thick layers of semiconductor alloys is constant throughout the frequency range, $0.1<f<10$ MHz. For InGaP, InGaAs, and SiGe, however, Λ increases monotonically as the frequency decreases from 10 to 0.6 MHz and remains approximately constant for frequency less than 0.6 MHz. The thermal conductivity of InGaAs measured at low frequencies ($\sim$6.2 W m^{-1} K^{-1}) is comparable to the thermal conductivity of a 1600 nm InGaAs thin film ($\sim$5.5 W m^{-1} K^{-1}) measured using the 3ω method[5] and thermal conductivity of a bulk sample ($\sim$6.4 W m^{-1} K^{-1}) derived from a thermal diffusivity measurement.[20] We note that an early study reported thermal conductivity of bulk InGaAs as $\sim$4.8 W m^{-1} K^{-1} measured by steady-state heating.[21]

We have also measured the thermal conductivity of several samples of InGaP and InGaAs where the thickness h of epitaxial alloy layers are much thinner than the $h=2010$ nm InGaP and $h=3330$ nm InGaAs layers discussed above. Data for thinner layers are compared to the frequency dependence of thick layers in Fig. 4. To create a common x axis for this plot, we convert the modulation frequency to a thermal penetration depth $\boldsymbol{d}$, defined as the depth from the sample surface where the temperature is e^{-1} of surface temperature, $\boldsymbol{d}=\sqrt{\Lambda/\pi Cf}$. The dependence of Λ on h and $\boldsymbol{d}$ is remarkably similar, see Fig. 4.

To gain qualitative insight into the mechanisms that underlie our experimental findings, we construct a simple isotropic continuum model describing lattice thermal conductivity, following the work of Morelli *et al.*[22] In this model, the phonon dispersion is isotropic and linear. We treat the longitudinal and transverse modes separately, and as explained in Ref. 22, we set the cutoff frequencies by the acoustic phonon frequencies at the zone boundary[14] to take into account only acoustic phonons up to the maximum frequencies at zone boundary. The speed of sound and cutoff frequencies used in the model are derived from the phonon dispersion in the [100] direction. We assume the Grüneisen constants, γ_L and γ_T, to be 1.0 and 0.7 for all crystals and alloys, and obtain the longitudinal and transverse phonon velocities, v_L and v_T of the crystals from Refs. 14, and use the average values for the alloys. As we have done previously,[23] we deviate from the approach of Ref. 22 and substitute a high temperature form for the N-process relaxation rate $\tau_N^{-1}=B_N\omega^2T$. We fix the relative anharmonic scattering strengths of umklapp and normal processes, B_U and B_N, by Eqs. 11(b), 12(b), and (25) of Ref. 22, and obtain absolute values of the anharmonic scattering strengths from fits to the thermal conductivities[14] of the crystals and virtual crystals (for alloys). This analysis yields $B_U^L=1.7$ for GaAs, 1.0 for InP, 2.1 for InGaAs, and 0.8 for InGaP, in units of 10^{-19} s K^{-1}. We calculate the strength of Rayleigh scattering in InGaP and InGaAs alloys using the dimensionless parameter Γ, see Eq. (16) of Ref. 22, that describes the strength of phonon scattering by mass disorder. We do not consider Rayleigh scattering by the differences in atomic size or bond strength because these contributions to Γ are not well known and, in any case, should oppose each other so that the total correction to Γ is relatively small.[23] We

derive $\Gamma_{InGaP}=0.0675$ and $\Gamma_{InGaAs}=0.0357$. We note that there is only one free parameter in our model, the absolute values of the anharmonic scattering strengths.

The dashed line in Fig. 4 shows the results of this model calculation for Λ with one additional phonon scattering rate $\tau^{-1}=v/h$ or, equivalently for this plot, $\tau^{-1}=v/\boldsymbol{d}$. Given the approximate form of the model, the agreement between this model and the data is satisfactory and suggests that a scattering rate of this form captures the essential physics of the experiment. This scattering rate has the form of phonon boundary scattering, in which phonons are assumed to be scattered at the interface between the thin films and the substrates. This assumption is reasonable for many combinations of thin films and substrates, but for an electronic grade epitaxial alloy, it is difficult to identify a mechanism that would strongly scatter low-frequency phonons at the interface since the film is only differentiated from the substrate by composition. The difference between the acoustic impedance of the epitaxial layer and the substrate is small and the structural perfection and chemical purity of the interfaces should be very high. And, of course, in the case of the frequency dependence of the thick layers, no physical interface exists at the penetration depth $\boldsymbol{d}$.

Instead, we propose that the boundary scattering form is able to describe the data because phonons with mean free paths $\ell > h$ or $\ell > \boldsymbol{d}$ do not contribute to the thermal conductivity of the alloy layer as measured in the experiment. Phonons with $\ell > h$ or $\ell > \boldsymbol{d}$ can be said to be "ballistic" on the length scale of the experiments.[24,25]

To understand this result, we must return to the details of the experiment. In a TDTR experiment, the sample is heated at the surface and the thermal response of the sample is measured at the surface and used to determine the thermal properties. Therefore, to capture the basic geometry of the experiment, consider one-dimensional heat flow in a semi-infinite solid that is subjected to a periodic heat source at the surface of $P\sin(2\pi ft)$, where P is the power per unit area. The steady-state temperature oscillation is then[26]

$$\Delta T = P\exp(-x/\boldsymbol{d})\sin(2\pi ft - \pi/4 - x/\boldsymbol{d})/\sqrt{\Lambda C 2\pi f}, \quad (1)$$

where x is the depth from sample surface, $\sqrt{\Lambda C}$ is the thermal effusivity, and $\boldsymbol{d}=\sqrt{\Lambda/\pi Cf}$ as defined before. We divide the contribution to the heat transport into two channels: a diffusive channel that incorporates all equilibrium phonons with $\ell < \boldsymbol{d}$ and a ballistic channel incorporating all nonequilibrium phonons with $\ell > \boldsymbol{d}$. The overall thermal effusivity is then the sum of the thermal effusivities of each channel rather than the thermal effusivity that would result from the sum of the thermal conductivities of the two channels. However, as the population of ballistics phonons consists of low-frequency phonons with small number of available modes, the heat capacity of the ballistic phonons is very small. Consequently, the thermal effusivity of the ballistic channel is also very small and does not contribute to the thermal conductivity determined by TDTR.

The striking similarity between the dependence of Λ on the thickness of thin layers and the frequency dependent Λ of thick layers is further illustrated in Fig. 5 where we plot the data and the model calculations as a function of temperature T. We label each set of data in this plot by the layer thickness h or penetration depth $\boldsymbol{d}$, whichever smaller. When $\boldsymbol{d} < h$, thermal conductivity of the epitaxial layers with comparable $\boldsymbol{d}$ coincides despite differences in layer thickness as large as an order of magnitude. The agreement between the model calculations with the measurements is reasonably good across the entire temperature range, giving further support to our conclusion that phonons with mean free paths longer than penetration depth do not contribute to the thermal conductivity measured by TDTR.

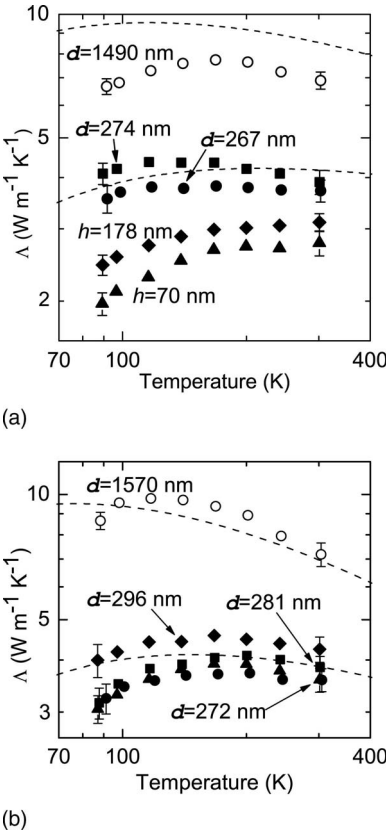

FIG. 5. (a) Temperature dependence of the thermal conductivity of InGaP epitaxial layers of thicknesses 2010 nm (circles), 456 nm (squares), 178 nm (diamonds), and 70 nm (triangles). (b) Temperature dependence of the thermal conductivity of InGaAs epitaxial layers of thicknesses 3330 nm (circles), 891 nm (squares), 591 nm (diamonds), and 431 nm (triangles). Both plots include measurements at modulation frequencies of 10 MHz (solid symbols) and 0.6 MHz (open symbols). The data sets are labeled by either the layer thickness h or the penetration depth at room temperature $\boldsymbol{d}$, whichever is smaller. The upper and lower dashed lines in each figure are thermal conductivities calculated using the isotropic continuum model described in the text that limits the mean free path of the phonons to either 1 μm or 100 nm, respectively.

Thermal conductivity distribution as a function of mean free path $\kappa(\ell)$ is readily derived from the frequency dependent measurements. The distribution function $\kappa(\ell)$ is defined by $\Lambda=\int\kappa(\ell)d\ell$. We approximate $\kappa(\ell)$ from the finite differences of the thermal conductivity with respect to penetration depth $\boldsymbol{d}$.

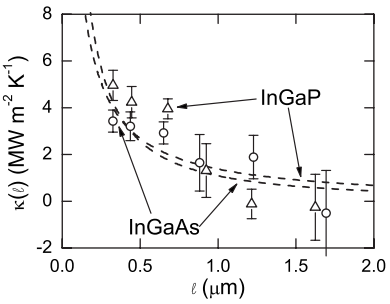

FIG. 6. Thermal conductivity distribution $\kappa(\ell)$ as a function of mean free path, ℓ. $\kappa(\ell)$ is defined by $\Lambda=\int\kappa(\ell)d\ell$. The open symbols are $\kappa(\ell)$ converted from frequency dependent measurements. The dashed lines are calculations from the isotropic continuum model described in the text. Error bars on the data points reflect the experimental uncertainties in the determination of $\kappa(\ell)$. The major source of experimental uncertainty is the setting of the absolute value of the phase of the reference channel of the rf lock-in amplifier and, at the lowest modulation frequencies, the correction needed to account for the optical pulses that leak through the pulse picker. The precision of the thermal conductivity measurements is approximately 1% at modulation frequencies of 10 MHz, 7% at 0.6 MHz, and 10% at 350 kHz.

$$\kappa(\ell)=\frac{d\Lambda}{d\ell}\approx\frac{\Lambda_{n+1}-\Lambda_n}{\boldsymbol{d}_{n+1}-\boldsymbol{d}_n}, \tag{2}$$

where Λ_{n+1} and Λ_n are the thermal conductivities measured at two adjacent modulation frequencies, and $\boldsymbol{d}_{n+1}$ and $\boldsymbol{d}_n$ are the corresponding penetration depths. The thermal conductivity distribution of InGaAs and InGaP derived using this approach is plotted in Fig. 6 using $\kappa(\ell)$ from Eq. (2) and $\ell=(\boldsymbol{d}_{n+1}+\boldsymbol{d}_n)/2$.

IV. SUMMARY

In summary, we report in this paper experimental evidence of frequency dependence of thermal conductivity in epitaxial semiconductor alloys. We demonstrate that the frequency dependence is fundamentally related to the thickness dependence of the epitaxial layers, as phonons of mean free paths longer than the penetration depth traverse the temperature gradient ballistically and do not contribute to the thermal conductivity measured by the experiment. Hence, frequency dependent measurements can be a convenient method for probing the phonon distributions of materials.

ACKNOWLEDGMENTS

This work was supported by ONR Grant No. N00014-05-1-0250. We thank Epiworks, Inc. for providing InGaP and InGaAs samples, M. Feng of UIUC for a multilayer HBT InGaP/GaAs wafer, and E. A. Fitzgerald of MIT for the $Si_{0.4}Ge_{0.6}$ sample. Sample characterization used the facilities of the Center of Microanalysis of Materials which is partially supported by the U.S. Department of Energy under Grant No. DEFG02-91ER45439, and Laser Facility of the Frederick Seitz Materials Research Laboratory (MRL) at UIUC.

[1] D. G. Cahill and R. O. Pohl, Annu. Rev. Phys. Chem. **39**, 93 (1988).
[2] P. G. Klemens, Phys. Rev. **119**, 507 (1960).
[3] D. Li, Y. Wu, P. Kim, L. Shi, P. Yang, and A. Majumdar, Appl. Phys. Lett. **83**, 2934 (2003).
[4] J. C. Caylor, K. Coonley, J. Stuart, T. Colpitts, and R. Venkatasubramanian, Appl. Phys. Lett. **87**, 023105 (2005).
[5] W. Kim, J. Zide, A. Gossard, D. Klenov, S. Stemmer, A. Shakouri, and A. Majumdar, Phys. Rev. Lett. **96**, 045901 (2006).
[6] Y. S. Ju and K. E. Goodson, Appl. Phys. Lett. **74**, 3005 (1999).
[7] G. D. Mahan and F. Claro, Phys. Rev. B **38**, 1963 (1988).
[8] R. A. Guyer and J. A. Krumhansl, Phys. Rev. **148**, 766 (1966).
[9] S. G. Volz, Phys. Rev. Lett. **87**, 074301 (2001).
[10] M. Feng, N. Holonyak, Jr., G. Walter, and R. Chan, Appl. Phys. Lett. **87**, 131103 (2005).
[11] W. Hafez and M. Feng, Appl. Phys. Lett. **86**, 152101 (2005).
[12] B. Ishaug, W.-Y. Hwang, J. Um, B. Guo, H. Lee, and C.-H. Lin, Appl. Phys. Lett. **79**, 1745 (2001).
[13] C. W. Leitz, M. T. Currie, A. Y. Kim, J. Lai, E. Robbins, E. A. Fitzgerald, and M. T. Bulsara, J. Appl. Phys. **90**, 2730 (2001).
[14] *Physics of Group IV Elements and II-V Compounds*, Landolt-Börnstein, Vol. 17, Pt. A, edited by O. Madelung (Springer-Verlag, Berlin, 1982).
[15] D. G. Cahill and F. Watanabe, Phys. Rev. B **70**, 235322 (2004).
[16] C. A. Paddock and G. L. Eesley, J. Appl. Phys. **60**, 285 (1986).
[17] D. A. Young, C. Thomsen, H. T. Grahn, H. J. Maris, and J. Tauc, in *Phonon Scattering in Condensed Matter*, edited by A. C. Anderson and J. P. Wolfe (Springer, Berlin, 1986), p. 49.
[18] D. G. Cahill, W. K. Ford, K. E. Goodson, G. D. Mahan, A. Majumdar, H. J. Maris, R. Merlin, and S. R. Phillpot, J. Appl. Phys. **93**, 793 (2003).
[19] D. G. Cahill, Rev. Sci. Instrum. **75**, 5119 (2004).
[20] E. F. Hockings, I. Kudman, T. E. Seidel, C. M. Schmelz, and E. F. Steigmeier, J. Appl. Phys. **37**, 2879 (1966).
[21] M. S. Abrahams, R. Braunstein, and F. D. Rosi, J. Phys. Chem. Solids **10**, 204 (1959).
[22] D. T. Morelli, J. P. Heremans, and G. A. Slack, Phys. Rev. B **66**, 195304 (2002).
[23] D. G. Cahill, F. Watanabe, A. Rockett, and C. B. Vining, Phys. Rev. B **71**, 235202 (2005).
[24] P. G. Sverdrup, S. Sinha, M. Asheghi, S. Uma, and K. E. Goodson, Appl. Phys. Lett. **78**, 3331 (2001).
[25] H.-Y. Chiu, V. V. Deshpande, H. W. Ch. Postma, C. N. Lau, C. Mikó, L. Forró, and M. Bockrath, Phys. Rev. Lett. **95**, 226101 (2005).
[26] H. S. Carslaw and J. C. Jaeger, *Conduction of Heat in Solids* (Oxford University Press, Oxford, 1959), p. 76.